

# LEVEL-SET SHAPE OPTIMIZATION VIA POLYTOPIC DISCONTINUOUS GALERKIN METHODS \*

RAPHAEL S. FERNANDES<sup>†</sup>, EMMANUIL H. GEORGOULIS<sup>‡</sup>, AND ALBERTO PAGANINI<sup>§</sup>

**Abstract.** We introduce a new level-set shape optimization approach based on polytopic (i.e., polygonal in two and polyhedral in three spatial dimensions) discontinuous Galerkin methods. The approach benefits from the geometric mesh flexibility of polytopic discontinuous Galerkin methods to resolve the zero-level set accurately and efficiently. Additionally, we employ suitable Runge-Kutta discontinuous Galerkin methods to update the level-set function on a fine underlying simplicial mesh. We discuss the construction and implementation of the approach, explaining how to modify shape derivative formulas to compute consistent shape gradient approximations using discontinuous Galerkin methods, and how to recover dG functions into smoother ones. Numerical experiments on unconstrained and PDE-constrained test cases evidence the good properties of the proposed methodology.

**Key words.** Shape optimization, level-set method, discontinuous Galerkin, polygonal and/or polyhedral elements, finite elements

**MSC codes.** 49M41, 49Q10, 65M60, 65N30

**1. Introduction.** The level-set method is a very popular shape optimization methodology based on the implicit representation of domain boundaries (shapes) as zero-level sets of a scalar function, which is often referred to simply as the *level-set function*. The level-set method has been successfully applied in a large variety of scenarios including structural mechanics, architecture, and multi-physics systems [2, 16, 25], among others. A notable feature of the level-set shape optimization methodology, which certainly contributed to its widespread use, is that this method is capable of performing also topological changes such as shape splitting or merging [2]. In particular, topological changes can occur even when level-set function updates are driven only by shape derivatives, which encode information of diffeomorphic (and thus non-topological) domain changes [19]. Of course, level-set optimization methods based on topological derivatives are also available [4, 8].

The level-set shape optimization methodology has been described in review and introductory articles [2, 32], and it has been implemented in open-source libraries [3, 44, 50]. Although many different variants exist, the method typically involves solving a *shape-gradient equation* to extract a descent direction from the shape derivative, and a *level-set equation* to update the level-set function. The shape-gradient equation is an elliptic boundary value problem with the shape derivative as right-hand side. The level-set equation is a transport partial differential equation (PDE) with non constant velocity (specifically, the shape gradient multiplied by -1). If the shape optimization

---

\*

**Funding:** The work of R. S. Fernandes is supported by the EPSRC DTP grant EP/V520172/1. E. H. Georgoulis wishes to acknowledge the financial support of EPSRC (grant number EP/W005840/2) and of The Leverhulme Trust (grant number RPG-2021-238).

<sup>†</sup>School of Computing and Mathematical Sciences, University of Leicester, Leicester LE1 7RH, United Kingdom ([rsf14@leicester.ac.uk](mailto:rsf14@leicester.ac.uk))

<sup>‡</sup>The Maxwell Institute for Mathematical Sciences & Department of Mathematics, School of Mathematical and Computer Sciences, Heriot-Watt University, Edinburgh EH14 4AS, United Kingdom, AND Department of Mathematics, School of Applied Mathematics and Physical Sciences, National Technical University of Athens, Zografou Campus, Athens 15780, Greece, AND IACM-FORTH, Crete 70013, Greece ([e.georgoulis@hw.ac.uk](mailto:e.georgoulis@hw.ac.uk))

<sup>§</sup>School of Computing and Mathematical Sciences, University of Leicester, Leicester LE1 7RH, United Kingdom ([a.paganini@leicester.ac.uk](mailto:a.paganini@leicester.ac.uk))

problem is constrained to partial differential equations, then determining the shape derivative also requires solving *state* and *adjoint equations* [19]. In some instances, e.g., in self-adjoint problems (but not only), the solution to the adjoint equation can be obtained by rescaling the solution to the state equation [2].

Solving PDE-constrained shape optimization problems with the level-set method generally requires three ingredients. The first one is a numerical method to solve the level-set equation, which is typically stated on a bounded domain containing shapes, often referred to as the *hold-all domain*. The second ingredient is a numerical method to solve the shape-gradient equation, whose right-hand side is supported on the domain implicitly represented by the level-set function. The third one is a numerical method to solve the state and the adjoint equations, which are defined on the domain implicitly represented by the level-set function.

The level-set equation is commonly solved using finite difference schemes on Cartesian grids [32]; these schemes typically require level-set reinitialization to ensure stability [36]. Another popular approach is to add diffusion to the level-set equation (in the spirit of vanishing viscosity [24]) and, subsequently, employ standard conforming piecewise-linear finite elements [40, 44]. In [9], the authors introduce an alternative method based on the method of characteristics and simplicial mesh adaptation, which is applied to level-set shape optimization in [1].

Solving the shape gradient, state, and adjoint equations is more challenging because these are partly or entirely defined on the domain implicitly represented by the level-set function. Since this is usually not resolved by the hold-all domain mesh, naively employing standard finite element methods leads to substantial discretization errors. Numerous approaches have been developed to address this issue. These can be classified as either being “unfitted” or “fitted” depending on how accurately they resolve the zero-level set.

Unfitted methods employ techniques to perform all computations on the hold-all domain mesh. A very popular unfitted method is the so-called “Ersatz material” approach [2], which recasts the state equation onto the hold-all domain by extending the equation’s coefficients in a suitable fashion. In this case, the shape gradient and the adjoint equations are also naturally reformulated on the hold-all domain. When applicable, this approach allows computing numerical solutions using standard finite element methods. However, the main drawback of the Ersatz material approach is that the zero-level set is not resolved accurately. Beside limiting computational accuracy, this drawback disqualifies the Ersatz material approach for problems where a precise description of the zero-level set is required as, for instance, in interface problems [1, 41]. These issues can be addressed by employing more sophisticated unfitted method like the CutFEM [7, 10], the XFEM [22, 34, 49], or the finite cell method [35, 43], among others.

Fitted methods employ techniques to accurately represent the implicitly defined domain. Classical examples are based on mesh adaptation [53], global re-meshing [52], or local re-meshing with mesh adaptation [1]. These approaches are effective, but can require careful case-by-case treatment and mesh management to prevent the mesh quality from deteriorating. In this work, we present a new fitted level-set shape optimization method that drastically simplifies the mesh management step by employing discontinuous Galerkin finite elements on polytopic meshes.

Polytopic meshes have been proved effective in shape and topology optimization thanks to their increased geometric flexibility. Polytopic Voronoi meshes with low-order conforming finite elements [30, 45, 46] or virtual elements [5, 28, 48] have been applied successfully in combination with the “Solid Isotropic Material with Penal-

ization” (SIMP) model. In the SIMP model, the state equation is extended to the hold-all domain similarly to the Ersatz material approach. Polytopic Voronoi meshes with low-order conforming finite elements have also been applied to the level-set shape optimization method with “Ersatz material” approach [51].

Polytopic meshes also greatly simplify fitted methods. In [37, 38], the authors discretize the level-set function using standard finite elements on hexahedral meshes, truncate the hexahedra with the zero-level set to generate a fitted polytopic mesh, employ modified trilinear and moving-least squares basis functions to compute the state, and solve the level-set equation using “essentially non-oscillatory” (ENO) schemes. In [27], the authors present a level-set shape optimization based on the topological derivative and generate fitted polytopic meshes by intersecting an initial Voronoi tessellation with the zero-level set. The state equation is solved using the symmetric Interior Penalty discontinuous Galerkin (IPdG) method on the polytopic mesh. The level-set equation is regularized by adding a small regularizing amount of diffusion and is solved on the polygonal Voronoi mesh using a symmetric IPdG method. This approach does not include the equivalent of the shape gradient equation because the topological derivative is applied pointwise. A different approach is presented in [17], where the authors combine polytopic meshes induced by a Laguerre diagram with the virtual element method and realized a shape and topology optimization method by acting directly on the Laguerre diagram parameters.

These works demonstrated some of the advantages polytopic meshes offer in the context of shape optimization such as higher element anisotropy or facilitated local refinement. However, polytopic methods have much more to offer. The last ten years or so have seen the development of a rich theory (supported by efficient implementations) of discontinuous Galerkin (dG) methods on general, possibly curved, polytopic elements [11–14, 21]. In particular, the element-wise discontinuous nature of the approximations spaces permitted by dG methods allows for extremely general element shapes. The ability to use elements of essentially arbitrary shape with the same number of local numerical degrees of freedom as those used on simplicial elements [12–14] effectively decouples the element shape from its approximation capabilities. This is extremely attractive in the context of shape optimization, since coarse polytopic elements can accurately represent complex shapes, in contrast to what is possible with coarse simplicial meshes. Moreover, hanging nodes are naturally embedded in the polytopic mesh paradigm.

In this work, we build on this enhanced geometric flexibility. Specifically, we propose a *polytopic discontinuous Galerkin framework* for fitted level-set shape optimization based on agglomeration of elements of a fine underlying simplicial mesh. The approach allows decoupling the discretization of the level-set equation, the discretization of the shape gradient equation, and the discretization of the state (and adjoint) equations. This approach streamlines and facilitates the construction of coarse agglomerated polytopic elements that *fit the zero-level set to great accuracy* and that, in combination with higher-order dG methods, allow the rapid solution of the shape gradient and of the state equations. Transferring information between a coarse polytopic mesh and the underlying fine simplicial mesh is also straightforward. This enables solving the level-set equation on the fine underlying simplicial mesh using standard, explicit, and stable Runge-Kutta dG (RKdG) methods, to a computational cost comparable to that of solving the shape gradient equation. We note that in [36] the authors evidence that using RKdG methods for the level-set equation in divergence form is very efficient, accurate, stable. Additionally, in contrast to Hamilton-Jacobi ENO methods, RKdG methods do not require non-standard procedures such as reini-

tialization. In this work, we apply RKdG methods directly to the level-set equation in non-divergence form, without any observed detrimental effect to the stability of the method.

The remainder of this work is organized as follows. In [section 2](#), we briefly review the level-set shape optimization method. In [section 3](#), we discuss the discontinuous Galerkin approximation of the shape gradient, the state, and the level-set equation, paying extra care to the consistent evaluation of the shape derivative on discontinuous test functions. In [section 4](#), we present a selection of numerical experiments that demonstrate the efficacy of the new method. We consider both unconstrained and PDE-constrained shape optimization test cases and use a steepest-descent optimization algorithm with backtracking and Armijo stopping rule. The method is implemented in Python and the code is available on the Zenodo archive at [\[26\]](#). Finally, in [section 5](#) we draw conclusions and outline future research directions.

**2. The level-set shape optimization method.** We review briefly the level-set shape optimization method; for an extensive introduction to the topic; we refer to the educational articles [\[2, 32\]](#).

Let  $D \subset \mathbb{R}^d$ ,  $d \in \mathbb{N}$ , be a fixed and Lipschitz hold-all domain. The level-set shape optimization method is based on the idea that to each continuous function  $\phi : D \rightarrow \mathbb{R}$  we can associate a domain

$$\Omega_\phi := \{x \in D : \phi(x) < 0\}.$$

This identification allows modifying both the shape and the topology of a domain  $\Omega_\phi$  by acting on the defining function  $\phi$ . For example, [Figure 2.1](#) shows that adding a negative constant to a function  $\phi$  can lead to changes in the shape and topology of  $\Omega_\phi$ .

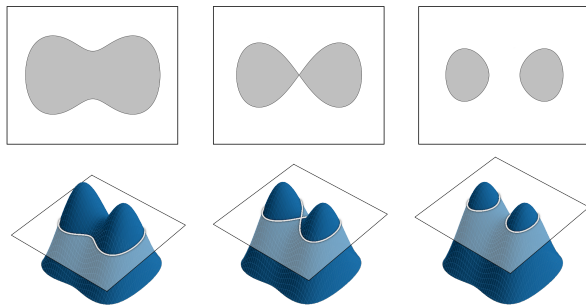


FIG. 2.1. Surf plot of a function  $\phi$  and zero level sets of  $\phi + c$ , where  $c$  is a negative constant (decreasing from left to right). Note that the shape and topology of  $\Omega_{\phi+c}$  changes depending on the value of  $c$ .

Let  $W^{1,\infty}(D, \mathbb{R}^d)$  denote the space of Lipschitz continuous functions with values in  $\mathbb{R}^d$ . For a fixed function  $V \in W^{1,\infty}(D, \mathbb{R}^d)$  with  $V = 0$  on  $\partial D$  and for  $\epsilon > 0$  sufficiently small, we consider the family of bi-Lipschitz bijections  $\{T_t : D \rightarrow D\}_{0 \leq t \leq \epsilon}$  defined by  $T_t(x) = x + tV(x)$  for all  $x$  in  $D$ . By applying  $T_t$  to  $\Omega_\phi$ , we can create a family of domains  $\Omega_\phi(t) := T_t(\Omega_\phi)$ . In turn, we can create a family of functions  $\{\varphi(t) : D \rightarrow \mathbb{R}\}_{0 \leq t \leq \epsilon}$  such that  $\Omega_{\varphi(t)} = \Omega_\phi(t)$  by simply defining  $\varphi(t, T_t(x)) = \phi(x)$  for all  $x$  in  $D$  and all  $0 \leq t \leq \epsilon$ . We henceforth refer to the variable  $t$  as “time”. By computing the total derivative of  $\varphi(t, T_t)$  with respect to  $t$ , we observe that  $\varphi$  is characterized by the hyperbolic initial value problem commonly known as *level-set*

equation:

$$(2.1) \quad \partial_t \varphi + V \cdot \nabla \varphi = 0 \quad \text{for } t \in (0, \epsilon), \quad \varphi(0) = \phi.$$

Let  $J : D \supset \Omega \mapsto J(\Omega) \in \mathbb{R}$  denote a sufficiently regular objective function. Using the level-set characterization (2.1), we can formulate a level-set shape optimization method to tackle the shape optimization problem:

$$\text{Find } \Omega \subset D \text{ such that } \Omega \in \underset{A \subset D}{\operatorname{argmin}} J(A).$$

More precisely, given an initial guess  $\Omega_\phi$ , we can generate a sequence of functions  $\phi^k$  such that  $J(\Omega_{\phi^k})$  is decreasing by setting  $\phi^0 = \phi$  and  $\phi^{k+1} := \varphi^k(t^k)$  for  $k \geq 0$ , where  $\varphi^k$  is the solution to

$$(2.2) \quad \partial_t \varphi^k - \nabla J(\Omega_{\phi^k}) \cdot \nabla \varphi^k = 0 \quad \text{for } t \in (0, \epsilon_k), \quad \varphi^k(0) = \phi^k,$$

$\nabla J(\Omega_{\phi^k})$  is the shape gradient of  $J$  at  $\Omega_{\phi^k}$  with respect to a suitable inner product, and  $\epsilon_k > 0$  and  $t^k \in (0, \epsilon_k)$  are suitable final and stopping times, respectively. Of course, the optimization algorithm is stopped if  $\nabla J(\Omega_{\phi^k}) = 0$ , in which case  $\phi^k$  is a stationary point. We recall that the shape derivative  $J$  at  $\Omega$  in the direction  $V \in W^{1,\infty}(D, \mathbb{R}^d)$  is given by

$$dJ(\Omega; V) := \lim_{t \rightarrow 0} \frac{J(T_t(\Omega)) - J(\Omega)}{t}.$$

Let  $(\mathcal{H}, (\cdot, \cdot)_{\mathcal{H}})$  be a Hilbert space of vector-valued functions defined over  $D$  such that  $W^{1,\infty}(D, \mathbb{R}^d)$  is dense in  $\mathcal{H}$ . In practice, a popular choice is to select  $\mathcal{H} = H_0^1(D, \mathbb{R}^d)$ , the space of  $\mathbb{R}^d$ -valued functions with components in  $H_0^1(D)$ , either endowed with the standard  $H^1$ - or the  $H_0^1$ -inner products, or an inner product stemming from the linear elasticity equations. Then, the shape gradient  $\nabla J(\Omega) \in \mathcal{H}$  of  $J$  at  $\Omega$  with respect to  $\mathcal{H}$  is the solution to

$$(2.3) \quad (\nabla J(\Omega), V)_{\mathcal{H}} = dJ(\Omega; V) \quad \text{for all } V \in \mathcal{H}.$$

For existence and uniqueness of a weak solution to (2.1), it is sufficient to assume that  $V \in W^{1,\infty}(D)$  and, in particular, the same is required for  $V = -\nabla J(\Omega_{\phi^k})$ . Since  $\nabla J(\Omega_{\phi^k})$  will be approximated by a Galerkin method over piecewise polynomial spaces, these approximations to  $\nabla J(\Omega_{\phi^k})$  will be bounded in  $D$  with piecewise bounded derivatives. Therefore, for existence and uniqueness of solution to (2.2), it is sufficient to ensure the global continuity of the approximations to  $\nabla J(\Omega_{\phi^k})$  inserted in (2.2).

*Example 2.1.* As a driving example, let  $f \in W^{1,1}(D)$  be a given scalar function, and let  $J(\Omega) := \int_{\Omega} f \, dx$ . Then, the shape derivative of  $J$  at  $\Omega \subset D$  in the direction  $V \in W^{1,\infty}(D, \mathbb{R}^d)$  is given by

$$dJ(\Omega; V) = \int_{\Omega} (\nabla f \cdot V + f \operatorname{div} V) \, dx.$$

*Remark 2.2.* As described in [18], it is also possible to compute steepest descent directions in  $W^{1,\infty}(D, \mathbb{R}^d)$ . These descent directions can be used to drive the evolution of the level-set function  $\varphi^k$  in (2.2) instead of using the negative shape gradient  $-\nabla J(\Omega_{\phi^k})$ . To the best of our understanding, computing such descent directions may

be computationally more involved than solving (2.3). Although we are not aware of their use in level-set based shape optimization, in other frameworks it has been observed that  $W^{1,\infty}(D, \mathbb{R}^d)$ -steepest direction based methods can outperform Hilbert space-based counterparts, especially when optimizing domains with corners. Since a comparison between different choices of descent directions is not the focus of this work, for simplicity we compute descent directions by solving (2.3). We highlight that, as presented below, the shape gradient equation (2.3) can be solved efficiently using polytopic meshes due to their reduction of computational complexity.

**3. Numerical level-set shape optimization using dG methods.** The numerical realization of the level-set shape optimization method (2.2) requires, at the very least, the discretization of the level set equation (2.1) and of the shape gradient equation (2.3). A very popular approach is to employ finite differences to solve (2.1) in combination with a standard conforming Galerkin method to solve (2.3). Instead, here we develop a *polytopic discontinuous Galerkin method* framework. The so-called *polytopic* (i.e., polygonal for  $d = 2$  or polyhedral for  $d = 3$ ) discontinuous Galerkin methods have been developed to be able to operate on meshes comprising essentially arbitrary element shapes. In [11–14], it has been shown that it is possible to construct *stable* discontinuous Galerkin methods on such extreme mesh scenarios. A pertinent feature of these methods is that the cardinality of the local elemental degrees of freedom are *independent* of the element shape, that is element geometry and number of faces/edges/vertices. This feature is naturally very attractive for shape optimization frameworks, whereby it is extremely important to strike a balance between total computational complexity, by using as coarse mesh as possible, and geometric feature resolution. As we shall see below, by allowing meshes with elements with essentially arbitrary shapes, we can follow zero-level sets with extremely high fidelity without requiring highly locally refined meshes in the zero-level set neighborhoods.

Before proceeding further, we recall some standard notation to introduce the discontinuous Galerkin method. To this end, let  $\mathcal{T}$  be a partition of the hold-all domain  $D$  into general polytopic elements. We consider the broken Sobolev space

$$H^1(\mathcal{T}) := \{v \in L^1(D) : v|_T \in H^1(T) \text{ for all } T \in \mathcal{T}\},$$

along with the broken gradient defined by  $(\nabla_h v)|_T := \nabla(v|_T)$ ,  $T \in \mathcal{T}$ . For a generic element  $T \in \mathcal{T}$ , let  $P_p(T)$  denote the space of tensor-product polynomials defined over  $T$ . We consider the element-wise (discontinuous) polynomial space

$$(3.1) \quad S_{\mathcal{T}}^p := \{v \in L^2(D) : v|_T \in P_p(T) \text{ for all } T \in \mathcal{T}\}.$$

and we denote by  $[S_{\mathcal{T}}^p]^d$  the space of vector-valued functions whose  $d$  components lie in  $S_{\mathcal{T}}^p$ . For later use we also consider the restriction  $S_{\mathcal{T},\Omega}^p$  of  $S_{\mathcal{T}}^p$  onto the domain  $\Omega \subset D$  given by

$$(3.2) \quad S_{\mathcal{T},\Omega}^p := \{v \in L^2(\Omega) : v|_{T \cap \Omega} \in P_p(T \cap \Omega) \text{ for all } T \in \mathcal{T}\},$$

and we denote the standard, orthogonal  $L^2(\Omega)$ -projection  $\Pi_{\Omega} : L^2(\Omega) \rightarrow S_{\mathcal{T},\Omega}^p$  onto  $S_{\mathcal{T},\Omega}^p$ , defined for every  $v \in L^2(\Omega)$  by

$$(3.3) \quad \int_{\Omega} (v - \Pi_{\Omega} v) w \, dx = 0 \quad \text{for all } w \in S_{\mathcal{T},\Omega}^p.$$

Finally, we recall the standard definitions of jump and averages of a function in  $S_{\mathcal{T}}^p$ . To this end, we introduce the notation  $\Gamma := \cup_{T \in \mathcal{T}} \partial T$  to denote the skeleton of the partition  $\mathcal{T}$ , and we define  $\Gamma_{\text{int}} := \Gamma \setminus \partial D$  and  $\Gamma_{\text{ext}} := \Gamma \cap \partial D$ .

DEFINITION 3.1. Let  $T^+$  and  $T^-$  be two neighboring elements, and let  $e := \partial T^+ \cap \partial T^- \in \Gamma_{int}$ . Let  $n^+$  and  $n^-$  denote the outward pointing unit normal vector fields on  $e$  with respect to  $T^+$  and  $T^-$ . Let  $\psi \in H^1(\mathcal{T})$  be a scalar function, and let  $\psi^+$  and  $\psi^-$  denote the traces onto  $e$  of  $\psi|_{T^+}$  and  $\psi|_{T^-}$ , respectively. The average  $\{\psi\}|_e$  and the jump  $[[\psi]]|_e$  of  $\psi$  on  $e$  are defined by

$$(3.4) \quad \{\psi\}|_e := \frac{1}{2}(\psi^+ + \psi^-) \quad \text{and} \quad [[\psi]]|_e := \psi^+ n^+ + \psi^- n^-,$$

respectively. Similarly, let  $\Psi \in [H^1(\mathcal{T})]^d$  be a vector valued function, and let  $\Psi^+$  and  $\Psi^-$  denote the traces onto  $e$  of  $\Psi|_{T^+}$  and  $\Psi|_{T^-}$ , respectively. The average  $\{\Psi\}|_e$  and the jump  $[[\Psi]]|_e$  of  $\Psi$  on  $e$  are defined by,

$$(3.5) \quad \{\Psi\}|_e := \frac{1}{2}(\Psi^+ + \Psi^-) \quad \text{and} \quad [[\Psi]]|_e := \Psi^+ \cdot n^+ + \Psi^- \cdot n^-,$$

respectively. Finally, let  $\tilde{T} \in \mathcal{T}$  be such that  $\partial \tilde{T} \cap \partial D \neq \emptyset$ . Let  $\tilde{e} := \partial \tilde{T} \cap \partial D \subset \Gamma_{ext}$ , and let  $\tilde{n}$  denote the outward pointing unit vector field on  $\tilde{e}$ . Let  $\tilde{\psi}$  and  $\tilde{\Psi}$  denote the traces onto  $\tilde{e}$  of  $\psi|_{\tilde{T}}$  and  $\Psi|_{\tilde{T}}$ , respectively. Using this notation, we extend the definition of jump and average on  $\Gamma_{ext}$  as follows:

$$(3.6) \quad \{\psi\}|_e := \tilde{\psi}, \quad [[\psi]]|_e := \tilde{\psi} \tilde{n}, \quad \{\Psi\}|_e := \tilde{\Psi}, \quad [[\Psi]]|_e := \tilde{\Psi} \cdot \tilde{n}.$$

**3.1. Discontinuous Galerkin discretization of the shape gradient equation.** Let  $\mathcal{H} = H_0^1(D, \mathbb{R}^d)$  be endowed with the standard  $H^1$ -norm, let  $E_i, i = 1, \dots, d$  denote the canonical basis of  $\mathbb{R}^d$ , and let  $g_i := \nabla J(\Omega) \cdot E_i, i = 1, \dots, d$  denote the components of  $\nabla J(\Omega)$ . Then, the shape gradient equation (2.3) implies that each  $g_i \in H_0^1(D)$  is characterized by the variational problem

$$(3.7) \quad \int_D (\nabla g_i \cdot \nabla w + g_i w) dx = dJ(\Omega; w E_i) \quad \text{for all } w \in H_0^1(D).$$

To derive the dG discretization of (3.7), it is important to highlight that the shape derivative  $dJ(\Omega; V)$  generally depends both on the direction  $V$  and its Jacobian  $DV$ . For this reason, we introduce the notation

$$dJ_i(\Omega; w, \nabla w) := dJ(\Omega; w E_i).$$

We can now derive the dG discretization of (3.7). First, we note that each  $g_i \in H_0^1(D)$  is the unique minimizer of the functionals

$$F_i : H_0^1(D) \ni v \mapsto 0.5 \int_D (|\nabla v|^2 + v^2) dx - dJ_i(\Omega; v, \nabla v).$$

To facilitate consistency of differentiation the presence of element-wise discontinuous functions, we consider the, so-called, lifting operator  $R : H^1(\mathcal{T}) \rightarrow [S_{\mathcal{T}}^p]^d$ , defined by

$$(3.8) \quad \int_D R(v) \cdot w dx = - \int_{\Gamma} [[v]] \cdot \{w\} ds \quad \text{for all } w \in [S_{\mathcal{T}}^p]^d,$$

we refer to [6] for a discussion and properties. We define the following discretized version of  $F_i$ , reading  $F_i^h : S_{\mathcal{T}}^p \rightarrow \mathbb{R}$ ,

$$(3.9) \quad F_i^h(v) := \frac{1}{2} \int_D (|\nabla_h v + R(v)|^2 + v^2) dx + \frac{1}{2} \int_{\Gamma} \sigma |[[v]]|^2 ds - dJ_i(\Omega; v, \nabla_h v + R(v)),$$

with  $\sigma : \Gamma \rightarrow \mathbb{R}$  a non-negative function, to be defined precisely in [subsection 3.2](#), typically referred to as the *discontinuity-penalization parameter*. The minimizer  $g_{i,h} \in S_{\mathcal{T}}^p$  to the discrete functional [\(3.9\)](#) is characterized by  $dF_i^h(g_{i,h}, w) = 0$  for all  $w \in S_{\mathcal{T}}^p$ , and can thus be computed by solving the finite dimensional variational problem

$$\begin{aligned}
(3.10) \quad B(g_{i,h}, w) &:= \int_D (\nabla_h g_{i,h} \cdot \nabla_h w + g_{i,h} w) \, dx \\
&+ \int_{\Gamma} \left( \sigma \llbracket g_{i,h} \rrbracket \cdot \llbracket w \rrbracket - \llbracket w \rrbracket \cdot \{\nabla_h g_{i,h}\} - \llbracket g_{i,h} \rrbracket \cdot \{\nabla_h w + R(w)\} \right) \, ds \\
&= dJ_i(\Omega; w, \nabla_h w + R(w)) \quad \text{for all } w \in S_{\mathcal{T}}^p.
\end{aligned}$$

To bypass the requirement of computing the lifting of every test function in [\(3.10\)](#), it is possible to derive a “pure” interior penalty method by considering the alternative discretized version of  $F_i$ , reading

$$\begin{aligned}
(3.11) \quad \tilde{F}_i^h : S_{\mathcal{T}}^p \ni v \mapsto &\frac{1}{2} \int_D (|\nabla_h v|^2 + v^2) \, dx - \int_{\Gamma} \{\nabla_h v\} \cdot \llbracket v \rrbracket \, ds + \frac{1}{2} \int_{\Gamma} \sigma |\llbracket v \rrbracket|^2 \, ds \\
&- dJ_i(\Omega; v, \nabla_h v + R(v)).
\end{aligned}$$

Then, the minimizer  $\tilde{g}_{i,h} \in S_{\mathcal{T}}^p$  to the discrete functional [\(3.11\)](#) is characterized by  $d\tilde{F}_i^h(\tilde{g}_{i,h}, w) = 0$  for all  $w \in S_{\mathcal{T}}^p$ , that is,

$$\begin{aligned}
(3.12) \quad \tilde{B}(g_{i,h}, w) &:= \int_D (\nabla_h \tilde{g}_{i,h} \cdot \nabla_h w + g_{i,h} w) \, dx \\
&+ \int_{\Gamma} \left( \sigma \llbracket \tilde{g}_{i,h} \rrbracket \cdot \llbracket w \rrbracket - \llbracket w \rrbracket \cdot \{\nabla_h \tilde{g}_{i,h}\} - \llbracket \tilde{g}_{i,h} \rrbracket \cdot \{\nabla_h w\} \right) \, ds \\
&= dJ_i(\Omega; w, \nabla_h w + R(w)) \quad \text{for all } w \in S_{\mathcal{T}}^p.
\end{aligned}$$

*Example 3.2.* In [Example 2.1](#), we saw that if  $J(\Omega) := \int_{\Omega} f \, dx$  for a given scalar function  $f \in W^{1,1}(D)$ , then

$$(3.13) \quad dJ(\Omega; V) = \int_{\Omega} (\nabla f \cdot V + f \operatorname{div} V) \, dx \quad \text{for } V \in W^{1,\infty}(D; \mathbb{R}^d).$$

The extension of formula [\(3.13\)](#) to vector fields of the form  $V = wE_i$  with  $w \in S_{\mathcal{T}}^p$  reads

$$\begin{aligned}
(3.14) \quad dJ_i(\Omega; w, \nabla w + R(w)) &= \int_{\Omega} (\nabla f \cdot E_i) w \, dx + \int_{\Omega} f \nabla_h w \cdot E_i \, dx + \int_{\Omega} \Pi_{\Omega} f R(w) \cdot E_i \, dx \\
&= \int_{\Omega} (\nabla f \cdot E_i) w \, dx + \int_{\Omega} f \nabla_h w \cdot E_i \, dx - \int_{\Gamma \cap \Omega} \llbracket w \rrbracket \{\Pi_{\Omega} f E_i\} \, ds.
\end{aligned}$$

As we shall see in the numerical experiments in [section 4](#), general polytopic elements will be constructed via *agglomeration* from a finer simplicial subdivision of the hold-all domain  $D$ . This is particularly pertinent in the present context of shape optimization, as we shall see below, due to the flexibility it offers in capturing small geometrical features with relatively coarse elements. At the same time, however, constructing polytopic meshes via agglomeration may result into very irregular element shapes. To ensure the stability of the dG method, therefore, we resort into sophisticated choice of the discontinuity-penalization parameter  $\sigma$ , as derived and justified in [\[11, 13\]](#).

**3.2. The discontinuity-penalization parameter.** For completeness, we now give a precise formula for the discontinuity-penalization function  $\sigma$  appearing in the interior penalty discontinuous Galerkin (IP-dG) formulations above. The stability and error analysis of the IP-dG method under this choice of penalization, as well as a detailed discussion on the practical relevance of this choice, can be found in [11, 13].

The construction of a suitable discontinuity-penalization function  $\sigma$  begins with the concept of (finite simplicial) covering. Each polytopical element  $T \in \mathcal{T}$  can be covered by a finite family  $\mathcal{K}_T := \{K_j\}_{j=1}^m$  of  $m \in \mathbb{N}$  simplices  $K_j$ , i.e., we have  $T \subset \cup_{K_j \in \mathcal{K}_T} K_j$ . We refer to  $\mathcal{K}_T$  as a *covering* of  $T$ . Of course, many coverings with different cardinalities exist. For instance, any simplicial partition of  $T$  is a covering; equally, coverings with overlapping simplices also exist. We shall denote by  $\mathbb{K}_T$  the set of all such coverings.

For a generic domain  $\omega \subset \mathbb{R}^s$ ,  $s \in \{1, \dots, d\}$ , let  $h_\omega$ ,  $\rho_\omega$  and  $|\omega|$  denote the diameter, the inscribed radius, and the  $sD$ -volume of  $\omega$ , respectively.

**DEFINITION 3.3.** *We say that an element  $T$  is  $p$ -coverable if there exists at least one covering  $\mathcal{K}_T$  of  $T$  such that*

$$\max_{x \in T} \left\{ \min_{z \in \partial K_j} |x - z| \right\} \leq \rho_{K_j} / (8p)^2,$$

with  $|\cdot|$  denoting the Euclidean distance, for some constants  $c_{sh} > 0$  and  $c'_{sh} > 0$ , such that  $c_{sh}^{-1} h_T \leq h_{K_j} \leq c_{sh} h_T$ , and  $(c'_{sh})^{-1} \rho_T \leq \rho_{K_j} \leq c'_{sh} \rho_T$ ,  $c'_{sh} > 0$ , for all  $K_j \in \mathcal{K}_T$ .

In other words, an element is  $p$ -coverable if there exists a covering  $\mathcal{K}_T$  comprising simplices each with similar shape-regularity to the original polytopical element  $T$ , which cover  $T$  within a distance at most  $\rho_{K_j} / (8p)^2$  each, away from the element's boundary  $\partial T$ . In [11], a considerably weaker concept of  $p$ -coverability is used allowing, in particular,  $K_j$  to be general *curved* prisms.

Let  $e \subset \Gamma_{\text{int}}$  denote a common face shared by two neighboring polytopical elements  $T^+, T^- \in \mathcal{T}$ . Let  $\mathbb{K}_T^e$  denote the set of all simplices that are contained in  $T$  and that contain  $e$  as part of a face. We define the restriction of the discontinuity-penalization parameter  $\sigma$  on  $e$  by

$$(3.15) \quad \sigma|_e := C_\sigma \max_{T \in \{T^+, T^-\}} \left\{ \min \left\{ \frac{|T|}{\sup_{K \in \mathbb{K}_T^e} |K|}, C_{\text{cov}}(T) \right\} \frac{p_T^2 |e|}{|T|} \right\}$$

for a computable constant  $C_\sigma > 0$ , depending on  $c_{sh}$  and on  $c'_{sh}$ , and where we set  $C_{\text{cov}}(T) := p_T^{2(d-1)}$  if  $T$  is  $p$ -coverable, or  $C_{\text{cov}}(T) := \infty$  if  $T$  is not  $p$ -coverable. The definition of the discontinuity-penalization parameter  $\sigma$  can be naturally extended to boundary faces  $e \subset \partial D \cap T$  for a  $T \in \mathcal{T}$  as follows

$$(3.16) \quad \sigma|_e := C_\sigma \min \left\{ \frac{|T|}{\sup_{K \in \mathbb{K}_T^e} |K|}, C_{\text{cov}}(T) \right\} \frac{p_T^2 |e|}{|T|}.$$

*Remark 3.4.* It is possible to extend this definition for extreme local element size and polynomial degree variations in the context of Robust IP-dG methods [20]; we refrain from doing so in the present work, preferring to focus on the shape-optimization aspects.

The definition of  $\sigma$  given in formulas (3.15) and (3.16) is designed for maximum generality. However, it may appear at first sight to be complicated to be implemented

in practice. If we additionally assume that each element  $T \in \mathcal{T}$  is star-shaped with respect to a ball  $B(x_0, ch_T)$  for some  $c < 1$  and  $x_0 \in T$ , then it is sufficient to select

$$\sigma|_e := C_\sigma \max_{T \in \{T_1, T_2\}} \{p_T^2 |e| h_T^{-d}\} \quad \text{and} \quad \sigma|_e := C_\sigma p_T^2 |e| h_T^{-d},$$

respectively.

**3.3. Recovery.** The requirement  $V \in [W^{1,\infty}(D)]^d$  in (2.1) is sufficient for the well-posedness of the respective PDE problem. However, (3.10) and (3.12) produce element-wise *discontinuous* approximations  $g_{i,h} \in S_{\mathcal{T}}^p$ . A natural and minimally invasive approach to address this is to perform local recovery of the vector field  $(g_{i,h})_{i=1}^d$  into  $H_0^1(D)$ . For this purpose, it is sufficient to perform a simple nodal averaging approach upon constructing a suitable sub-division of the polytopic elements into  $d$ -dimensional simplices.

More specifically, we consider  $\tilde{\mathcal{T}}$  to be a refinement of  $\mathcal{T}$  into simplices, meaning that each polytopic element  $T \in \mathcal{T}$  is subdivided into  $r_T$  simplices  $\tau_m \subset T$  with  $m = 1, \dots, r_T$ , so that  $\bar{T} = \cup_{m=1}^{r_T} \bar{\tau}_m$ . (The same, or different simplicial subdivision of each polytopic element can be used for quadrature computations during assembly, see also [13, 21].) Related to the simplicial mesh  $\tilde{\mathcal{T}}$ , we consider the discontinuous element-wise polynomial space

$$(3.17) \quad S_{\tilde{\mathcal{T}}}^p := \{v \in L^2(D) : v|_\tau \in P_p(\tau) \text{ for all } \tau \in \tilde{\mathcal{T}}\},$$

for which we have, trivially,  $S_{\tilde{\mathcal{T}}}^p \subset S_{\mathcal{T}}^p$ . We also denote by  $\tilde{\Gamma}$  the skeleton of  $\tilde{\mathcal{T}}$ . Further, on  $S_{\tilde{\mathcal{T}}}^p$ , for each Lagrange node  $x_j$  of each element  $\tau$ , globally numbered via  $j = 1, \dots, \dim S_{\tilde{\mathcal{T}}}^p$ , we consider the nodal element patch  $\omega(x_j) := \{\tau \in \tilde{\mathcal{T}} : x_j \in \bar{\tau}\}$ , with cardinality denoted by  $\text{card}(\omega(x_j))$ . We define the nodal averaging recovery operator  $\mathcal{E} : S_{\tilde{\mathcal{T}}}^p \rightarrow H^1(D) \cap S_{\mathcal{T}}^p$  by

$$\mathcal{E}(v)(x_j) := \frac{1}{\text{card}(\omega(x_j))} \sum_{\tau \in \omega(x_j)} v|_\tau(x_j)$$

for  $v \in S_{\tilde{\mathcal{T}}}^p$  and  $x_j \in D$ , while  $\mathcal{E}(v)(x_j) = 0$  for all  $x_j \in \partial D$ . Note that if a Lagrangian node  $x_j$  lies in the interior of a simplex  $\tau$ , then  $\mathcal{E}(w)(x_j) = w(x_j)$ , because in this case  $\omega(x_j) = \tau$ .

With this, by solving (3.10) or (3.12), injecting the numerical solution into  $S_{\tilde{\mathcal{T}}}^p$ , and applying recovery operator  $\mathcal{E}$ , we obtain an approximate shape gradient  $\nabla J(\Omega)_h \in [S_{\tilde{\mathcal{T}}}^p \cap H_0^1(D)]^d$ . Note that, since  $\nabla J(\Omega)_{\tilde{h}}$  is continuous and element-wise polynomial, we also have  $\nabla J(\Omega)_{\tilde{h}} \in [W^{1,\infty}(D)]^d$ .

*Remark 3.5.* A completely analogous construction is possible when the fine mesh  $\tilde{\mathcal{T}}$  comprises box-type elements, i.e., quadrilaterals when  $d = 2$  or hexahedra for  $d = 3$ . The only modification is that the respective recovery space is then the space of element-wise mapped tensor-product elements, as is standard in conforming finite elements.

**3.4. Runge-Kutta discontinuous Galerkin discretization of the level-set equation.** Having constructed a recovered  $\nabla J(\Omega)_h \in [W^{1,\infty}(D)]^d$ , we consider the level-set equation (2.1) with  $V = -\nabla J(\Omega)_h$ . To approximate its solution  $\varphi$  on  $D$ , we employ a Runge-Kutta discontinuous Galerkin (RKdG) method for first order equations on a simplicial (or box-type) mesh  $\mathcal{T}^{fine}$ , i.e., a refinement into simplicial

(or box-type) elements of the polytopic mesh  $\mathcal{T}$ . For instance, we may take  $\mathcal{T}^{fine} = \tilde{\mathcal{T}}$  as in [subsection 3.3](#), or we could even consider  $\mathcal{T}^{fine}$  to be a refinement of  $\tilde{\mathcal{T}}$ . For notational simplicity, we shall, henceforth, take  $\mathcal{T}^{fine} = \tilde{\mathcal{T}}$ , stressing that this is not necessary for the overall framework to work.

We note that, employing a spatial discretization of [\(2.1\)](#) on  $\tilde{\mathcal{T}}$  (or a refinement thereof!), is *not* necessarily detrimental to the overall complexity of the method. This is due to the explicit time-stepping nature of RKdG, since no global linear system is required to be solved on each time-step, and since quadratures take place on simplicial subdivisions. Indeed, the main computational cost (associated with the time-stepping component of an explicit RKdG method) consists in assembling elemental mass matrices and solving the resulting block-diagonal linear systems. Using  $L^2$ -orthogonal bases, which are available for simplices, the mass matrices become diagonal, making this computational costs negligible. Of course, it is by all means possible to employ general polytopic meshes for the discretization of the level-set equation [\[12\]](#). In this case, assembly of elemental mass matrices typically involves quadrature computations on a simplicial subdivision of the polytopic mesh, in which case the computational cost is the same as computing directly on the simplicial subdivision. For large problems, this can be significantly accelerated via GPU implementations [\[21\]](#). Using polytopic meshes may lead to fewer but larger blocks compared to a discretization on the underlying simplicial mesh. However, the resulting polytopic elemental mass matrices are generally not diagonal, and so the fast solution aspect may be compromised. We also note that the spatial accuracy is generally driven by elements' diameters, and so solutions computed on polytopic meshes may be less accurate than counterparts obtained on their simplicial subdivision. Therefore, given the comparable computational cost and potentially higher accuracy, we opt for solving the level-set equation on the simplicial subdivision  $\mathcal{T}$ .

For a generic element  $\tau \in \tilde{\mathcal{T}}$ , we denote by  $\partial\tau^-$  the inflow region of  $T$ , that is

$$(3.18) \quad \partial\tau^- := \{x \in \partial\tau : V \cdot n < 0\}.$$

Note that  $\partial\tau^- \subset \Gamma_{\text{int}}$  because  $V = -\nabla J(\Omega)_{\tilde{h}}$  vanishes on  $\partial D$  due to our choice of  $\mathcal{H}$  in [subsection 3.1](#).

For a sufficiently smooth function  $w : D \rightarrow \mathbb{R}$ , we define the so-called *upwind jump* at  $x \in \partial\tau^- \subset \Gamma_{\text{int}}$  to be

$$(3.19) \quad [w](x) := w^+(x) - w^-(x), \quad \text{where} \quad w(x)^\pm := \lim_{\epsilon \rightarrow 0^+} w(x \pm \epsilon V).$$

Let assume that the initial condition  $\phi$  lies in  $S_{\tilde{\mathcal{T}}}^p$  (otherwise,  $\phi$  can be just replaced by its  $L^2$ -projection  $\Pi_\Omega(\phi) \in S_{\tilde{\mathcal{T}}}^p$ ). The spatially discrete discontinuous Galerkin method for the level-set problem [\(2.1\)](#) on  $\tilde{\mathcal{T}}$  reads: find  $\varphi_{\tilde{h}} \in S_{\tilde{\mathcal{T}}}^p$  such that  $\varphi_{\tilde{h}}(0) = \phi$  in  $D$  and

$$(3.20) \quad \int_D (\varphi_{\tilde{h}})_t w \, dx + \sum_{\tau \in \tilde{\mathcal{T}}} \int_\tau (V \cdot \nabla \varphi_{\tilde{h}}) w \, dx - \sum_{\tau \in \tilde{\mathcal{T}}} \int_{\partial\tau^-} (V \cdot n) [\varphi_{\tilde{h}}] w^+ \, ds = 0 \quad \text{for all } w \in S_{\tilde{\mathcal{T}}}^p.$$

The spatially discrete dG method [\(3.20\)](#) does not include upwind boundary terms because  $V|_{\partial D} = 0$ .

Finally, we discretize [\(3.20\)](#) with respect to the  $t$ -variable using explicit Runge-Kutta methods that have favorable properties when combined with spatial dG discretizations. We briefly review these methods and their properties here for the sake of completeness.

Selecting a local elemental basis  $\{\psi_\tau^i\}_{i=1}^{\dim(P_p(\tau))}$ , we express the elemental mass and “stiffness” matrices as  $M_\tau := (m_{ij}^\tau)_{i,j=1}^{\dim(P_p(\tau))}$  and  $K_\tau := (k_{ij}^\tau)_{i,j=1}^{\dim(P_p(\tau))}$ , where

$$m_{ij}^\tau := \int_\tau \psi_T^j \psi_T^i dx \quad \text{and} \quad k_{ij}^\tau := \int_\tau (V \cdot \nabla \psi_T^j) \psi_T^i dx - \int_{\partial\tau \setminus \partial D^-} (V \cdot n) \left[ \psi_T^j \right] (\psi_T^i)^+ ds,$$

respectively. We note that, upon selecting orthogonal elemental basis, e.g., the so-called Dubiner system [31],  $M_\tau$  becomes diagonal, and thereby trivially invertible.

Let  $\varphi_{\tilde{h}}|_\tau(t) := \sum_{j=1}^{\dim(P_p(\tau))} \Phi_\tau^j(t) \psi_\tau^j$ , let  $\Phi_\tau(t) := (\Phi_\tau^1(t), \dots, \Phi_\tau^{\dim(P_p(\tau))}(t))$ , and let  $L_\tau := -M_\tau^{-1}K_\tau$ . With this notation, we can write (3.20) on each  $\tau \in \tilde{\mathcal{T}}$  as

$$(3.21) \quad \frac{d}{dt} \Phi_\tau(t) = L_\tau \Phi_\tau(t), \quad t \in (0, \epsilon),$$

On (3.21), we apply a standard stable Runge-Kutta method, such as such as Heun’s method, or TVB-type methods [15], selecting carefully the appropriate CFL restrictions.

**3.5. Polytopic dG discretization of the level-set shape optimization method.** We can now describe how to exploit the polytopic dG methods ability to simply and accurately resolve domain boundaries (the zero-level set) in the computation of the shape derivative and of eventual PDE constraints and adjoint equations. We first recall from subsection 3.4 that the level-set function  $\varphi$  is approximated on the simplicial mesh  $\tilde{\mathcal{T}}$  using a Runge-Kutta dG method. Since the approximation  $\varphi_{\tilde{h}}$  is discontinuous, we postprocess it with the recovery strategy described in subsection 3.3 to ensure that the implicitly defined domain  $\Omega_{\mathcal{E}(\varphi_{\tilde{h}})}$  is well defined. Then, we identify the simplices that intersect the zero level set by tracking the change of sign of  $\mathcal{E}(\varphi_{\tilde{h}})$  on the mesh nodes. For example, in 2D we mark the  $i^{\text{th}}$  triangle if

$$\left| \frac{\mathcal{E}(\varphi_{\tilde{h}})(x_{i,1})}{|\mathcal{E}(\varphi_{\tilde{h}})(x_{i,1})|} + \frac{\mathcal{E}(\varphi_{\tilde{h}})(x_{i,2})}{|\mathcal{E}(\varphi_{\tilde{h}})(x_{i,2})|} + \frac{\mathcal{E}(\varphi_{\tilde{h}})(x_{i,3})}{|\mathcal{E}(\varphi_{\tilde{h}})(x_{i,3})|} \right| < 3,$$

where  $x_{i,1}, x_{i,2}$ , and  $x_{i,3}$  denote the triangle vertices. Here, we tacitly assume that if  $\mathcal{E}(\varphi_{\tilde{h}})$  is a piecewise polynomial of degree higher than one, then  $\tilde{\mathcal{T}}$  is sufficiently fine so that, e.g. in 2D, the recovered level-set function  $\mathcal{E}(\varphi_{\tilde{h}})$  does not change sign twice along any mesh edge.

After marking the simplices, we locally refine them to better resolve the zero-level set, thus creating a refined partition  $\mathcal{T}^{\text{ref}} \supset \tilde{\mathcal{T}}$  (see Figure 3.1 for an example in 2D). Finally, we agglomerate the simplices in  $\mathcal{T}^{\text{ref}}$  to form the polytopic subdivision  $\mathcal{T}^{\text{agg}} \subset \mathcal{T}^{\text{ref}}$ , which can be used to compute the approximation of the shape gradient as discussed in subsection 3.1. For example, in the numerical experiments presented in section 4, we create  $\mathcal{T}^{\text{agg}}$  using the following simple graph partitioning method based on  $k$ -means clustering [33]. First, we determine the barycenters of the triangles in  $\mathcal{T}^{\text{ref}}$  and interpret them as the set of observations  $\{x_j \in \mathbb{R}^2 : j = 1, \dots, n_{\text{ref}}\}$ , where  $n_{\text{ref}}$  denotes the number of simplices in  $\mathcal{T}^{\text{ref}}$ . Then, we split the set of observations in two depending on the sign of  $\phi(x_j)$  and introduce  $k^+ \in \mathbb{N}$  and  $k^- \in \mathbb{N}$  distributed sets  $C_i^+$  and  $C_i^-$ . We assign each barycenter  $x_j$  with  $\phi(x_j) > 0$  to a distributed set  $C_i^+$  by minimizing the quantity

$$\sum_{i=1}^{k^+} \sum_{x \in C_i^+} \left\| x - \frac{1}{|C_i^+|} \sum_{y \in C_i^+} y \right\|^2,$$

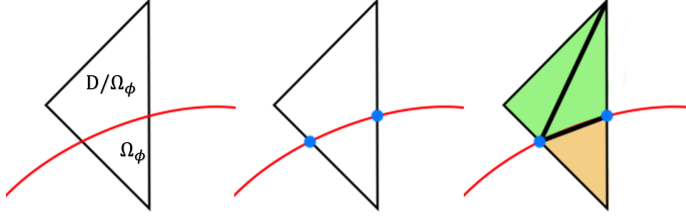


FIG. 3.1. *Example of local refinement method in 2D. Upon each edge that is intersected by the zero-level set  $\{\phi = 0\}$  (red curved line), we interpolate the level set function and determine its zeros, where we append new nodes (black dots) used to split the triangle in (at most) three subtriangles. To obtain a more accurate representation of the zero-level set, one could first subdivide elements that intersect the zero-level set and then apply the local refinement method to newly generated elements that intersect the zero-level set, possibly in combination with a higher-order moving-mesh shape optimization method [42].*

where  $|C_i^+|$  denotes the cardinality of  $C_i^+$  and  $\|\cdot\|$  denotes the Euclidean distance. Barycenters  $x_j$  with  $\phi(x_j) < 0$  are assigned to  $C_i^-$  in a similar fashion. Finally, we agglomerate triangles with barycenters in the same distributed set to form the  $(k^+ + k^-)$  polytopic elements in  $\mathcal{T}^{\text{agg}}$ . Examples of  $\tilde{\mathcal{T}}$ ,  $\mathcal{T}^{\text{ref}}$  and  $\mathcal{T}^{\text{agg}}$  can be seen in both [Figure 4.1](#) and [Figure 4.2](#).

We conclude this section by briefly explaining how to define and integrate polynomial basis functions on arbitrarily shaped polygonal elements. For a more detailed treatment of the polytopic dG finite element method, we refer to [\[13, 14\]](#).

The construction of basis functions on polytopic elements is based upon defining tensor-product polynomial spaces on each element using tightly fitting bounding boxes. Each bounding box is chosen such that the most extreme vertices of the polytope  $T$  align with the edges of the bounding box so that we acquire a minimum bounding box  $B_T$ . Upon this bounding box  $B_T$ , we can construct a set of basis functions by restricting onto  $T$  the tensor-product Legendre polynomials spanning  $P_p(T)$ .

To assemble the Galerkin matrices, we take advantage of the underlying simplicial mesh  $\mathcal{T}^{\text{ref}}$  used to form the polytopes  $T \in \mathcal{T}^{\text{agg}}$ . More specifically, we define quadrature schemes on polytopes by simply combining standard quadrature rules for simplexes.

**4. Numerical experiments.** We now demonstrate the good numerical performance of the level-set shape optimization method based on polytopic discontinuous Galerkin discretizations.

**4.1. Optimization algorithm.** As explained in [section 2](#), starting from an initial guess  $\Omega_{\phi^0}$ , we can generate a sequence of functions  $\phi^k$  such that  $J(\Omega_{\phi^k})$  is decreasing in a steepest-descent with line-search fashion [\[39\]](#). More specifically, we set  $\phi^{k+1} := \varphi^k(t^k)$  for  $k \geq 0$ , where:  $\varphi^k$  is a numerical solution to

$$(4.1) \quad \partial_t \varphi^k - \nabla J(\Omega_{\phi^k}) \cdot \nabla \varphi^k = 0 \quad \text{for } t \in (0, \epsilon_k), \quad \varphi^k(0) = \phi^k,$$

$t^k \in (0, \epsilon_k)$  is a suitable stopping time, and  $\nabla J(\Omega_{\phi^k})$  is a numerical solution to

$$(4.2) \quad (\nabla J(\Omega_{\phi^k}), V)_{\mathcal{H}} = dJ(\Omega_{\phi^k}; V) \quad \text{for all } V \in \mathcal{H},$$

for a chosen Hilbert space  $\mathcal{H}$ . In the following numerical experiments, we use  $\mathcal{H} = H_0^1(D; \mathbb{R}^d)$ , but other choices are possible. The final time  $\epsilon_k$  must be chosen such

that  $\varphi^k(t)$  exists for every  $t \in (0, \epsilon_k)$ . Note that both  $\epsilon_k$  and the time step  $\Delta t_k$  used to approximate  $\varphi^k$  depend on the  $W^{1,\infty}(D; \mathbb{R}^d)$ -norm of  $\nabla J(\Omega_{\phi^k})$ , which possibly changes at each iteration  $k$ . In the following numerical experiments, we select  $\Delta t_k$  to satisfy the CFL-condition and perform at most  $M \in \mathbb{N}$  time steps, thus implicitly setting  $\epsilon_k = M\Delta t_k$ . The stopping time  $t^k$  is selected in a backtracking fashion as the largest in the set  $\{5m\Delta t_k : m \in \mathbb{N}, 0 < 5m \leq M\}$  such that the Armijo condition

$$(4.3) \quad J(\Omega_{\varphi^k(m\Delta t_k)}) \leq J(\Omega_{\varphi^k(0)}) - c(m\Delta t_k) \|\nabla J(\Omega_{\phi^k})\|_{\mathcal{H}}^2$$

is satisfied, where the constant  $c \in (0, 1)$  is set to  $c = 0.01$ . The optimization algorithm is stopped after 80 iterations, or if the Armijo condition (4.3) is not satisfied after one time step, that is, if

$$J(\Omega_{\varphi^k(\Delta t_k)}) > J(\Omega_{\varphi^k(0)}) - c\Delta t_k \|\nabla J(\Omega_{\phi^k})\|_{\mathcal{H}}^2.$$

The workflow of the resulting optimization algorithm for unconstrained problems is sketched in Figure 4.1. Its extension to PDE-costrained problems is depicted in Figure 4.2. We anticipate that in these numerical experiments, as well as in every other we performed (not reported here), the level-set shape optimization algorithm based on the discontinuous Galerkin method did not require a reinitialiation of the level set function  $\phi$ , a procedure that is commonly invoked in the literature [1, 2, 47]. This is in agreement with the findings in [36] in the case the level-set equation in divergence form for divergence-free velocity vectors.

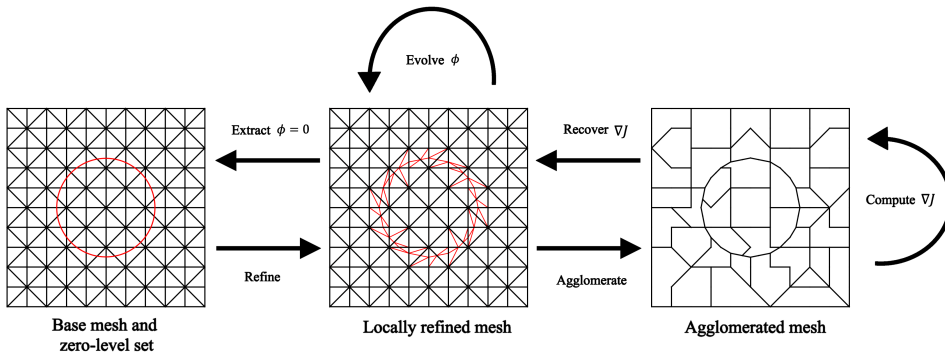


FIG. 4.1. Workflow of the agglomerated polytopic dG level-set shape optimization method. A base triangular mesh (left) is locally refined to better fit the zero-level set  $\phi = 0$ . The resulting mesh (middle) is subsequently agglomerated into a polytopic mesh (right) to compute an approximate solution to the shape gradient equation (4.2). The solution  $\nabla J$  is then recovered (via interpolation and nodal averaging) on the locally refined triangular mesh, where the level-set equation (4.1) is solved using a time-stepping scheme. When the time-stepping scheme stops, the base mesh is locally refined to better fit the zero-level set of the updated level-set function  $\phi$ . This procedure is repeated until the convergence or stopping criteria are met.

**4.2. Unconstrained test case.** We consider the unconstrained shape functional  $J(\Omega) := \int_{\Omega} f \, dx$ , where the bivariate function  $f$  is chosen as

$$f(x) := f(x_1, x_2) = \sqrt[4]{((x - 0.7)^2 + y^2)((x + 0.7)^2 + y^2)} - 0.6.$$

To solve the level-set equation (4.1), we partition the hold-all domain  $D$  into 1800 triangles, discretize in space using RKdG with spatial basis functions of degree

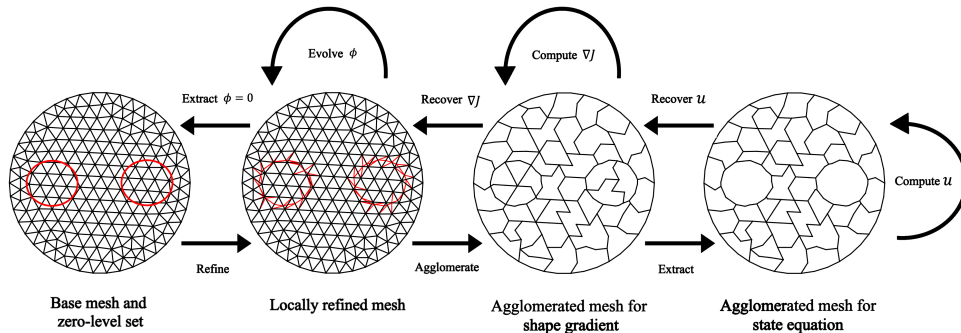


FIG. 4.2. Extension of the agglomerated polytopic dG level-set shape optimization workflow presented in Figure 4.1 to PDE-constrained shape optimization problems. The workflow begins as in Figure 4.1. To compute the shape gradient  $\nabla J$ , we first extract the state equation’s computational domain and compute the state solution  $u$ . The state solution is then recovered (via interpolation of  $u$ ,  $\nabla u$ , and the lift  $R(u)$ ) on the polytopic mesh used to compute the shape gradient  $\nabla J$ . Then, the workflow continues as in Figure 4.1.

$p = 2$  and timestepping via Heun’s method with time step  $\Delta t_k = 1/2600$ , with at most  $M = 150$  time steps per iteration. Choosing a very small time step  $\Delta t_k$  is not a requirement of the dG method employed. This choice is simply due to the desire to generate “smooth” convergence histories for plotting purposes and to provide a “smallest step” stopping criteria for the backtracking algorithm. To solve the shape gradient equation (4.2), we agglomerate the locally refined triangular mesh (cf. Figure 4.1) into 200 polytopic elements and employ polynomials of degree  $p = 2$ . Table 4.1 reports a numerical validation of the polytopic discontinuous Galerkin approximation of the shape gradient. The computation of the shape derivative  $dJ$  in the discontinuous Galerkin framework is discussed in Example 3.2, see (3.14). To assemble the various Galerkin matrices, we employ quadrature rules of order four both on triangles and on edges, which compute the involved integrals exactly (up to round-off errors).

TABLE 4.1

Numerical validation of the polytopic discontinuous Galerkin approximation of the shape gradient  $\nabla J$  in the unconstrained test case. The computational domain is a square of edge length 2 and the zero-level set is a circle of radius 0.52 (both centered at the origin, as depicted in white in the most left image in Figure 4.3). In the table, the index  $i$  denotes the level of refinement,  $N$  denotes the number of polytopic elements, and  $err_l$  and  $err_q$  denote the  $L^2$ -error for affine and quadratic polygonal finite element approximations, respectively. The approximate reference solution has been computed using standard continuous quadratic finite elements on a simplicial mesh with 4944 elements. We observe that the approximate algebraic converge rates computed using the formula  $rate(i) = \log(err(i)/err(i-1))/\log(N(i)/N(i-1))$  are close to  $-1$  and  $-1.5$ , which are the expected rates for finite element approximations based on affine and quadratic polynomials, respectively.

$i$	$N$	$err_l$	$rate_l$	$err_q$	$rate_q$
1	36	1.34e-3	-	3.09e-4	-
2	144	4.06e-4	-0.86	6.70e-5	-1.10
3	576	1.35e-4	-0.79	7.25e-6	-1.60
4	2304	3.86e-5	-0.91	1.04e-6	-1.40

Some shape iterates, starting from a disc of radius 0.51 centered at the origin, are displayed in Figure 4.3. The normalized pseudo-time evolution of the objective

function is depicted in Figure 4.5 We observe that the algorithm retrieves a good approximation of the optimal (and not connected) shape. To assess the advantage of the agglomerated polytopic dG approach to compute shape derivatives, we compare it with a more classical dG approach based on triangular meshes. For the latter, we also employ an adaptive quadrature based on locally refined meshes to evaluate the shape derivative formula  $dJ$  accurately on triangles that intersect the level-set boundary  $\phi = 0$ . For both methods, we solve the level-set equation (4.1) on a fine underlying simplicial mesh as in the previous numerical experiment. Figures 4.4 and 4.5 summarizes the qualitative and quantitative comparison between the two approaches when using 50, 200, and 450 triangular or polytopic elements. The quantitative comparison is performed both in terms of the objective functions  $J$  and a numerical approximation of the distance between zero-level sets defined as  $\max_{x \in \{\varphi=0\}} \min_{y \in \{f=0\}} |x - y|$ . We observe that the adaptive nature of the agglomerated polytopic approach allows it to achieve accurate results also with coarser meshes.

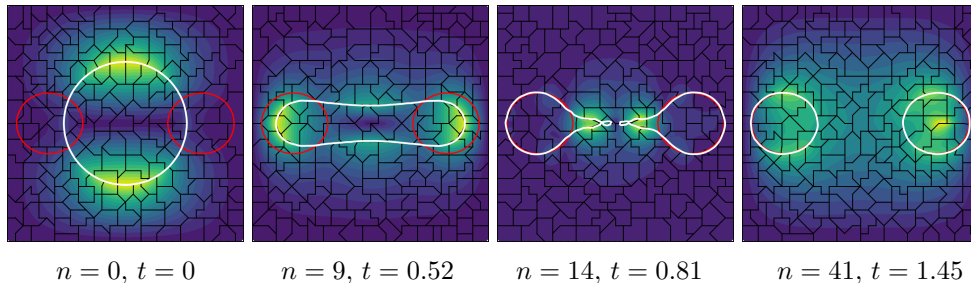


FIG. 4.3. Evolution of shapes for the unconstrained test case. The variables  $n$  and  $t$  denote the number of gradient evaluations and the pseudo-time, respectively. The initial domain, a disc (drawn in white), elongates and eventually splits into two domains before converging to the optimal configuration (drawn in red). The contour plots represent the normalized contours of the Euclidean norm of the gradient  $\nabla J$ . Note that the polytopic mesh changes at each iteration.

**4.3. PDE-constrained test case.** We consider the PDE-constrained objective function  $J(\Omega, u) := \int_{\Omega} \nabla u \cdot \nabla u + \eta^2 dx$ , where  $u \in H^1(\Omega)$  is the weak solution to

$$(4.4) \quad -\Delta u = 0 \quad \text{in } \Omega, \quad u = f \quad \text{on } \partial\Omega.$$

This PDE-constrained optimization problem stems from the class of Bernoulli free boundary value problems. In these problems, a part  $\Gamma_{\text{free}}$  of the boundary  $\Gamma$  is moved so that the solution  $u$  to the state problem (4.4) satisfies simultaneously both the Dirichlet and Neumann boundary conditions  $u = f$  and  $\partial_n u = \eta$  on  $\Gamma_{\text{free}}$  [23]. Specifically, we set the hold-all  $D$  to be a unit disc centered at the origin. The boundary  $\partial D$  of  $D$  coincides with the fixed part  $\Gamma_{\text{fixed}} := \Gamma \setminus \Gamma_{\text{free}}$  of the boundary  $\Gamma$ . The free boundary  $\Gamma_{\text{free}}$  is the boundary of subdomains compactly embedded in  $D$ . Furthermore, we set  $f = -1$  on  $\Gamma_{\text{fixed}}$ ,  $f = 0$  on  $\Gamma_{\text{free}}$ , and  $\eta = 1/(-0.55 \ln(0.55))$ , so that the optimal shape is an annulus with internal radius equal to 0.55. This data has been generated starting from the fact that, if  $\Omega$  is an annulus and  $f$  is constant on each connected component of  $\partial\Omega$ , then the solution to (4.4) is of the form  $u(x) = a \log(|x|) + b$ , where  $a, b \in \mathbb{R}$  are two constants that depend on the  $\Omega$  and  $f$ .

In this setting, the shape derivative of  $J$  in a sufficiently regular direction  $V$  is [29]:

$$(4.5) \quad dJ(\Omega, u; V) = \int_{\Omega} \nabla u \cdot (\text{div}(V) - DV^{\top} - DV) \nabla u + \eta^2 \text{div}(V) dx.$$

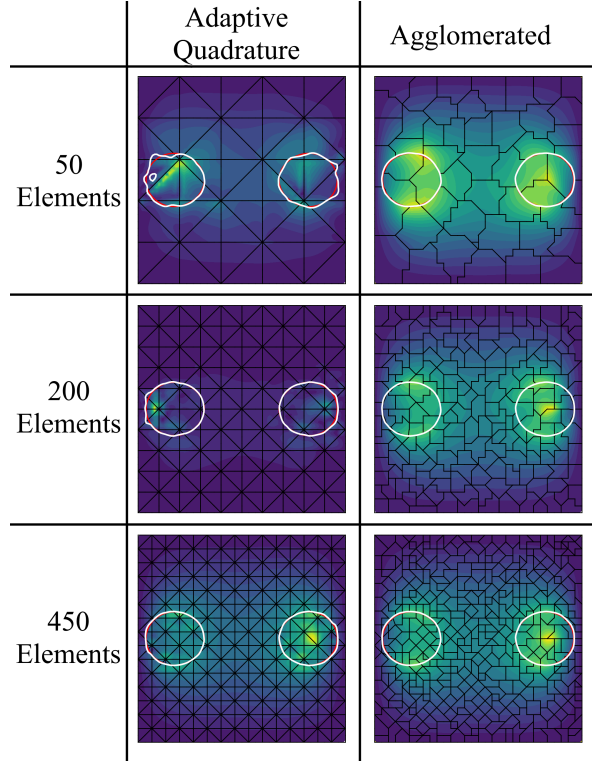


FIG. 4.4. Qualitative comparison (based on the unconstrained test case) between the agglomerated polytopic dG approach and a more classical approach based on triangular elements with adaptive quadrature. The optimal solution is the union of two disjoint disk-shaped domains depicted in red. The optimized shapes are depicted in white. The background shows the meshes employed and the normalized contours of the Euclidean norm of the gradient  $\nabla J$ . We observe that, as expected, both approaches retrieve increasingly accurate solutions as the the number of mesh elements increases. The agglomerated polytopic dG approach with 50 elements is qualitatively comparable, if not better, than the adaptive quadrature approach with 450 elements.

To extend formula (4.5) to directions of the form  $V = wE_i$ , where  $w \in S_{\mathcal{T}}^p$  and  $E_i$   $i = 1, \dots, d$  denotes the canonical basis of  $\mathbb{R}^d$ , we note that  $\operatorname{div}(V) = \nabla w \cdot E_i$ , and  $DV = E_i(\nabla w)^\top$ . Therefore,

$$\begin{aligned}
 dJ_i(\Omega, u; w, \nabla w + R(w)) &= \sum_{T \in \mathcal{T}} \int_{T \cap \Omega} \left( (\eta^2 + \nabla u \cdot \nabla u)(\nabla w + R(w)) \cdot E_i \right. \\
 &\quad \left. - \nabla u \cdot ((\nabla w + R(w))E_i^\top + E_i(\nabla w + R(w))^\top) \nabla u \right) dx.
 \end{aligned}$$

Using the definition of the lifting operator (3.8), since  $\eta^2 \in S_{\mathcal{T}}^p$ , we can rewrite

$$\sum_{T \in \mathcal{T}} \int_{T \cap \Omega} (\eta^2 + \nabla u \cdot \nabla u) R(w) \cdot E_i dx = - \int_{\Gamma_{\text{int}} \cap \bar{\Omega}} [[w]] \{ (\eta^2 + \nabla u \cdot \nabla u) E_i \} ds.$$

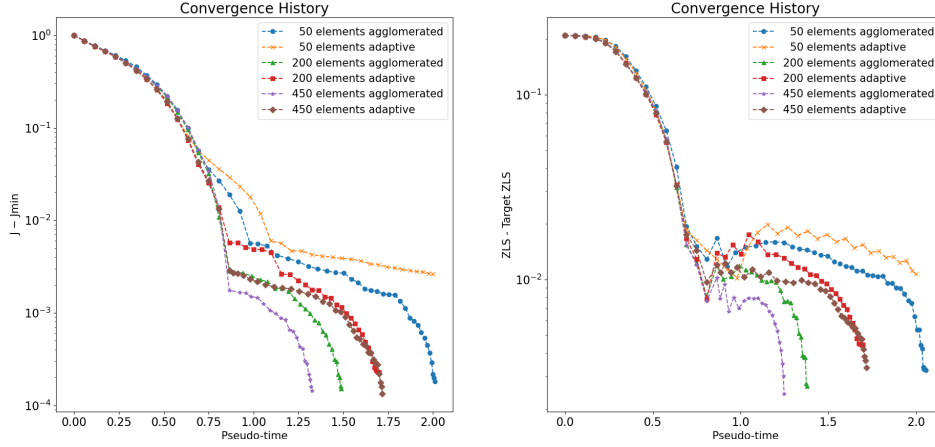


FIG. 4.5. *Quantitative comparison (based on the unconstrained test case) between the agglomerated polytopic dG approach and a more classical approach based on triangular elements with adaptive quadrature. The figure on the left depicts the pseudo-time evolution of the difference between the objective value  $J$  as shapes are optimized and (an accurate approximation of) the objective value at the optimal solution. The figure on the right depicts the pseudo-time evolution of an approximate distance between the zero-level set of the optimized shapes and the zero-level set of the optimal shape. Markers denote gradient evaluations. We observe that the agglomerated polytopic dG generally converges more rapidly and accurately than the adaptive quadrature approach.*

Similarly,

$$\begin{aligned} \sum_{T \in \mathcal{T}} \int_{T \cap \Omega} \nabla u \cdot (R(w)E_i^\top + E_i R(w)^\top) \nabla u \, dx &= \sum_{T \in \mathcal{T}} \int_{T \cap \Omega} 2(\nabla u \cdot E_i) \nabla u \cdot R(w) \, dx \\ &= - \int_{\Gamma_{\text{int}} \cap \bar{\Omega}} \llbracket w \rrbracket \{2(\nabla u \cdot E_i) \nabla u\} \, ds. \end{aligned}$$

Therefore, we conclude that

$$\begin{aligned} dJ_i(\Omega, u; w, \nabla w + R(w)) &= \sum_{T \in \mathcal{T}} \int_{T \cap \Omega} (\eta^2 + \nabla u \cdot \nabla u) E_i \cdot \nabla w - 2(\nabla u \cdot E_i) \nabla u \cdot \nabla w \, dx \\ &\quad - \int_{\Gamma_{\text{int}} \cap \bar{\Omega}} \llbracket w \rrbracket \{(\eta^2 + \nabla u \cdot \nabla u) E_i - 2(\nabla u \cdot E_i) \nabla u\} \, ds. \end{aligned}$$

Similarly as in [subsection 4.2](#), to solve the level-set equation [\(4.1\)](#), we partition the hold-all domain  $D$  into 2085 triangles, discretize in space using a classical dG method with basis functions of degree  $p = 2$ , and employ the Heun’s method (with time step  $\Delta t_k = 1/1000$ ) for time-stepping. Per iteration, we perform at most  $M = 100$  time steps. To solve the shape gradient equation [\(4.2\)](#) and the state equation [\(4.4\)](#), we agglomerate the locally refined triangular mesh (cf. [Figure 4.1](#)) into 200 polytopic elements and employ polynomials of degree  $p = 2$ . To assemble the various Galerkin matrices, we employ a quadrature rule of order 4 on triangles, an of order 4 on edges, which computes the involved integrals exactly (up to round-off errors). Note that, as displayed in [Figure 4.1](#), the state constraint is solved by extracting its computational domain instead of pursuing the so-called “Ersatz material” approach [\[2\]](#).

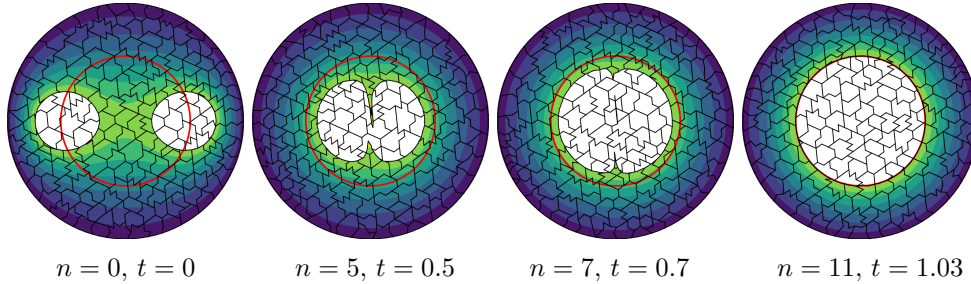


FIG. 4.6. Evolution of shapes for the PDE-constrained test case. The variables  $n$  and  $t$  denote the number of gradient evaluations and the pseudo-time, respectively. The two holes in the initial domain merge into one and then expand, converging to the optimal configuration (depicted in red). The contour plots represent the normalized contours of the Euclidean norm of the gradient  $\nabla J$ . Note that the polytopic mesh changes at each iteration.

Some shape iterates starting from

$$\phi(x) = \phi(x_1, x_2) = \sqrt[4]{((x - 0.6)^2 + y^2)((x + 0.6)^2 + y^2)} - 0.55,$$

are displayed in Figure 4.6. We observe that the algorithm retrieves a good approximation of the optimal shape. To demonstrate the generality of the approach, Figure 4.7 displays some shape iterates starting from a different initial guess. The convergence histories for both initial guesses are displayed in Figure 4.8.

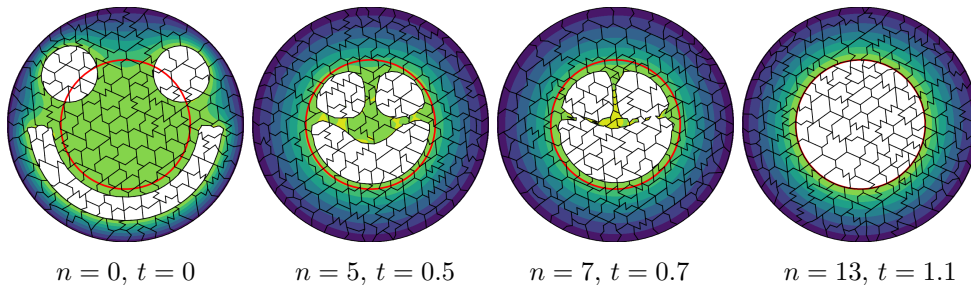


FIG. 4.7. Evolution of shapes for the PDE-constrained test case with a different initial guess. The variables  $n$  and  $t$  denote the number of gradient evaluations and the pseudo-time, respectively. The shape iterates happily converge to the optimal annular domain (depicted in red).

**5. Conclusions.** We have presented a new level-set shape optimization method based on polytopic discontinuous Galerkin discretizations. More specifically, the new shape optimization method exploits the geometric flexibility and robustness of polytopic dG methods, which allows computing with higher order polynomials defined on arbitrarily shaped polytopes that resolve the zero-level set accurately with no need for mesh adjustments. The method also takes advantage of the efficiency and stability of explicit Runge-Kutta discontinuous Galerkin methods to solve the level-set equation on a fine simplicial meshes, thus bypassing the need to reinitialize the level-set function.

We provided a detailed description of the method derivation and explained how to modify the evaluation of shape derivatives to compute consistent shape gradient approximations using discontinuous Galerkin methods. The numerical experiments evidenced the good performance of the method on unconstrained and PDE-constrained

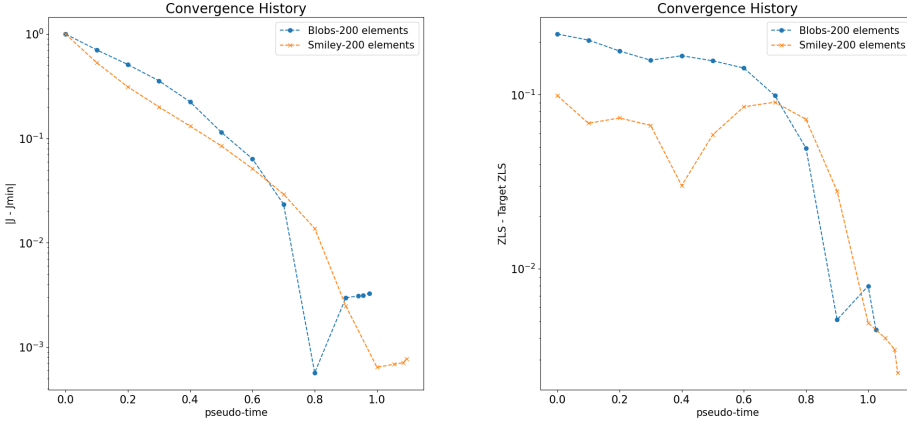


FIG. 4.8. Convergence history for the PDE-constrained test case with different initial guesses: one as in Figure 4.6 and one as in Figure 4.7. The figure on the left depicts the pseudo-time evolution of the difference between the objective value  $J$  as shapes are optimized and (an accurate approximation of) the objective value at the optimal solution. The figure on the right depicts the pseudo-time evolution of an approximate distance between the zero-level set of the optimized shapes and the zero-level set of the optimal shape. Markers denote gradient evaluations. We observe that both convergence measures are significantly reduced as optimization proceeds. The convergence lines in the plot on the left plateau due to numerical approximations errors leading to objective values  $J$  fictitiously smaller than objective value at the optimal solution.

test cases. An open-source Python implementation of the method is available on the Zenodo archive at [26].

Thanks to its flexibility in terms of element shapes, polynomial order, treatment of hanging nodes, stability, the method presented here is perfectly positioned for the development of a *posteriori* *hp*-adaptive shape optimization methods. The above developments can be combined with GPU-accelerated implementations of *hp*-version polytopic IPdG methods [21] to enable extremely fast solution of the RKdG step.

We note that, although the numerical experiments presented are based on two-dimensional shape optimization examples, three-dimensional problems can be treated using the same methodology, without the need of any further considerations. The favorable computational complexity observed is expected to be retained in the context of three-dimensional setting also. Finally, given the availability of interior penalty dG methods for various classes of PDE problems, the treatment of for more complex PDE problems is by all means possible.

## REFERENCES

- [1] G. ALLAIRE, C. DAPOGNY, AND P. FREY, *Shape optimization with a level set based mesh evolution method*, Computer Methods in Applied Mechanics and Engineering, 282 (2014), pp. 22–53, <https://doi.org/10.1016/j.cma.2014.08.028>.
- [2] G. ALLAIRE, C. DAPOGNY, AND F. JOUVE, *Chapter 1 - Shape and topology optimization*, in Geometric Partial Differential Equations - Part II, A. Bonito and R. H. Nochetto, eds., vol. 22 of Handbook of Numerical Analysis, Elsevier, 2021, pp. 1–132, <https://doi.org/10.1016/bs.hna.2020.10.004>.
- [3] G. ALLAIRE AND M. H. GFRERER, *AutoFreeFem: Automatic code generation with FreeFEM++ and LaTeX output for shape and topology optimization of non-linear multi-physics problems*, 2024, <https://arxiv.org/abs/2407.11713>.

- [4] S. AMSTUTZ AND H. ANDRÄ, *A new algorithm for topology optimization using a level-set method*, Journal of computational physics, 216 (2006), pp. 573–588.
- [5] P. ANTONIETTI, M. BRUGGI, S. SCACCHI, AND M. VERANI, *On the virtual element method for topology optimization on polygonal meshes: A numerical study*, Computers & Mathematics with Applications, 74 (2017), pp. 1091–1109, <https://doi.org/10.1016/j.camwa.2017.05.025>.
- [6] D. N. ARNOLD, F. BREZZI, B. COCKBURN, AND L. D. MARINI, *Unified analysis of discontinuous Galerkin methods for elliptic problems*, SIAM J. Numer. Anal., 39 (2001/02), pp. 1749–1779, <https://doi.org/10.1137/S0036142901384162>.
- [7] A. BERNLAND, E. WADBRO, AND M. BERGGREN, *Acoustic shape optimization using cut finite elements*, International Journal for Numerical Methods in Engineering, 113 (2018), pp. 432–449, <https://doi.org/10.1002/nme.5621>.
- [8] S. BLAUTH AND K. STURM, *Quasi-Newton methods for topology optimization using a level-set method*, Structural and Multidisciplinary Optimization, 66 (2023), p. 203.
- [9] C. BUI, C. DAPOGNY, AND P. FREY, *An accurate anisotropic adaptation method for solving the level set advection equation*, International Journal for Numerical Methods in Fluids, 70 (2012), pp. 899–922.
- [10] E. BURMAN, D. ELFVerson, P. HANSBO, M. G. LARSON, AND K. LARSSON, *Cut topology optimization for linear elasticity with coupling to parametric nondesign domain regions*, Comput. Methods Appl. Mech. Engrg., 350 (2019), pp. 462–479, <https://doi.org/10.1016/j.cma.2019.03.016>.
- [11] A. CANGIANI, Z. DONG, AND E. H. GEORGIOULIS, *hp-version discontinuous Galerkin methods on essentially arbitrarily-shaped elements*, Math. Comp., 91 (2021), pp. 1–35, <https://doi.org/10.1090/mcom/3667>.
- [12] A. CANGIANI, Z. DONG, E. H. GEORGIOULIS, AND P. HOUSTON, *hp-Version discontinuous Galerkin methods for advection-diffusion-reaction problems on polytopic meshes*, ESAIM: M2AN, 50 (2016), pp. 699–725, <https://doi.org/10.1051/m2an/2015059>.
- [13] A. CANGIANI, Z. DONG, E. H. GEORGIOULIS, AND P. HOUSTON, *hp-Version discontinuous Galerkin methods on polygonal and polyhedral meshes*, SpringerBriefs in Mathematics, Springer Cham, first ed., 2017.
- [14] A. CANGIANI, E. H. GEORGIOULIS, AND P. HOUSTON, *hp-Version discontinuous Galerkin methods on polygonal and polyhedral meshes*, Mathematical Models and Methods in Applied Sciences, 24 (2014), pp. 2009–2041, <https://doi.org/10.1142/S0218202514500146>.
- [15] B. COCKBURN AND C.-W. SHU, *TVB Runge-Kutta local projection discontinuous Galerkin finite element method for conservation laws. II. General framework*, Math. Comp., 52 (1989), pp. 411–435, <https://doi.org/10.2307/2008474>.
- [16] C. DAPOGNY, A. FAURE, G. MICHAELIDIS, G. ALLAIRE, A. COUVELAS, AND R. ESTEVEZ, *Geometric constraints for shape and topology optimization in architectural design*, Computational Mechanics, 59 (2017), pp. 933–965.
- [17] C. DAPOGNY, B. LEVY, AND E. OUDET, *A lagrangian shape and topology optimization framework based on semi-discrete optimal transport*, 2024, <https://arxiv.org/abs/2409.07873>, <https://arxiv.org/abs/2409.07873>.
- [18] DECKELNICK, KLAUS, HERBERT, PHILIP J., AND HINZE, MICHAEL, *A novel  $W^{1,\infty}$  approach to shape optimisation with Lipschitz domains*, ESAIM: COCV, 28 (2022), p. 2, <https://doi.org/10.1051/cocv/2021108>.
- [19] M. C. DELFOUR AND J.-P. ZOLÉSIO, *Shapes and geometries: metrics, analysis, differential calculus, and optimization*, no. DC22 in Advances in design and control, Society for Industrial and Applied Mathematics, Philadelphia, 2nd ed ed., 2011.
- [20] Z. DONG AND E. H. GEORGIOULIS, *Robust interior penalty discontinuous Galerkin methods*, J. Sci. Comput., 92 (2022), pp. Paper No. 57, 23, <https://doi.org/10.1007/s10915-022-01916-6>.
- [21] Z. DONG, E. H. GEORGIOULIS, AND T. KAPPAS, *GPU-accelerated discontinuous galerkin methods on polytopic meshes*, SIAM Journal on Scientific Computing, 43 (2021), pp. C312–C334, <https://doi.org/10.1137/20M1350984>.
- [22] P. DUYSINX, L. VAN MIEGROET, T. JACOBS, AND C. FLEURY, *Generalized shape optimization using X-FEM and level set methods*, in IUTAM Symposium on Topological Design Optimization of Structures, Machines and Materials, M. P. Bendsøe, N. Olhoff, and O. Sigmund, eds., Dordrecht, 2006, Springer Netherlands, pp. 23–32.
- [23] K. EPPLER AND H. HARBRECHT, *Shape optimization for free boundary problems—analysis and numerics*, in Constrained optimization and optimal control for partial differential equations, vol. 160 of Internat. Ser. Numer. Math., Birkhäuser/Springer Basel AG, Basel, 2012, pp. 277–288, [https://doi.org/10.1007/978-3-0348-0133-1\\_15](https://doi.org/10.1007/978-3-0348-0133-1_15).
- [24] L. C. EVANS, *Partial differential equations*, vol. 19, American Mathematical Society, 2022.

- [25] F. FEPPON, *Shape and topology optimization of multiphysics systems*, PhD thesis, Université Paris-Saclay (ComUE), 2019.
- [26] R. S. FERNANDES, E. H. GEORGIOULIS, AND A. PAGANINI, *Numerical implementation of a polytopic dG level-set shape optimization method in Python*, Apr. 2025, <https://doi.org/10.5281/zenodo.15193853>.
- [27] N. FERRO, S. MICHELETTI, N. PAROLINI, S. PEROTTO, M. VERANI, AND P. F. ANTONIETTI, *Level set-fitted polytopal meshes with application to structural topology optimization*, *Computers & Mathematics with Applications*, 169 (2024), pp. 99–111, <https://doi.org/10.1016/j.camwa.2024.06.011>.
- [28] A. L. GAIN, G. H. PAULINO, L. S. DUARTE, AND I. F. MENEZES, *Topology optimization using polytopes*, *Computer Methods in Applied Mechanics and Engineering*, 293 (2015), pp. 411–430, <https://doi.org/10.1016/j.cma.2015.05.007>.
- [29] R. HIPTMAIR AND A. PAGANINI, *Shape optimization by pursuing diffeomorphisms*, *Comput. Methods Appl. Math.*, 15 (2015), pp. 291–305, <https://doi.org/10.1515/cmam-2015-0013>.
- [30] T. Y. S. HOSHINA, I. F. M. MENEZES, AND A. PEREIRA, *A simple adaptive mesh refinement scheme for topology optimization using polygonal meshes*, *Journal of the Brazilian Society of Mechanical Sciences and Engineering*, 40 (2018), p. 348, <https://doi.org/10.1007/s40430-018-1267-5>.
- [31] G. E. KARNIADAKIS AND S. J. SHERWIN, *Spectral/hp element methods for computational fluid dynamics*, *Numerical Mathematics and Scientific Computation*, Oxford University Press, New York, second ed., 2005, <https://doi.org/10.1093/acprof:oso/9780198528692.001.0001>.
- [32] A. LAURAIN, *A level set-based structural optimization code using FEniCS*, *Struct. Multidiscip. Optim.*, 58 (2018), pp. 1311–1334, <https://doi.org/10.1007/s00158-018-1950-2>.
- [33] J. B. MACQUEEN, *Some methods for classification and analysis of multivariate observations*, in *Proceedings of the fifth Berkeley symposium on mathematical statistics and probability*, vol. 1, Oakland, CA, USA, 1967, pp. 281–297.
- [34] D. MAKHJIA AND K. MAUTE, *Numerical instabilities in level set topology optimization with the extended finite element method*, *Structural and Multidisciplinary Optimization*, 49 (2014), pp. 185–197, <https://doi.org/10.1007/s00158-013-0982-x>.
- [35] C. N. MALLON, A. W. THORNTON, M. R. HILL, AND S. BADIA, *Neural level set topology optimization using unfitted finite elements*, 2024, <https://arxiv.org/abs/2303.13672>.
- [36] E. MARCHANDISE, J.-F. REMACLE, AND N. CHEVAUGEON, *A quadrature-free discontinuous galerkin method for the level set equation*, *Journal of Computational Physics*, 212 (2006), pp. 338–357, <https://doi.org/10.1016/j.jcp.2005.07.006>.
- [37] S. H. NGUYEN AND H.-G. KIM, *Level set based shape optimization using trimmed hexahedral meshes*, *Computer Methods in Applied Mechanics and Engineering*, 345 (2019), pp. 555–583, <https://doi.org/10.1016/j.cma.2018.11.006>.
- [38] S. H. NGUYEN, D. SOHN, AND H.-G. KIM, *A novel hr-adaptive mesh refinement scheme for stress-constrained shape and topology optimization using level-set-based trimmed meshes*, *Structural and Multidisciplinary Optimization*, 65 (2022), p. 71, <https://doi.org/10.1007/s00158-021-03132-6>.
- [39] J. NOCEDAL AND S. J. WRIGHT, *Numerical optimization*, *Springer Series in Operations Research and Financial Engineering*, Springer, New York, second ed., 2006.
- [40] M. OTOMORI, T. YAMADA, K. IZUI, AND S. NISHIWAKI, *Matlab code for a level set-based topology optimization method using a reaction diffusion equation*, *Structural and Multidisciplinary Optimization*, 51 (2015), pp. 1159–1172, <https://doi.org/10.1007/s00158-014-1190-z>.
- [41] A. PAGANINI, *Approximate shape gradients for interface problems*, in *New Trends in Shape Optimization*, A. Pratelli and G. Leugering, eds., Cham, 2015, Springer International Publishing, pp. 217–227, [https://doi.org/10.1007/978-3-319-17563-8\\_9](https://doi.org/10.1007/978-3-319-17563-8_9).
- [42] A. PAGANINI, F. WECHSUNG, AND P. E. FARRELL, *Higher-order moving mesh methods for pde-constrained shape optimization*, *SIAM Journal on Scientific Computing*, 40 (2018), pp. A2356–A2382, <https://doi.org/10.1137/17M1133956>.
- [43] J. PARVIZIAN, A. DÜSTER, AND E. RANK, *Topology optimization using the finite cell method*, *Optimization and Engineering*, 13 (2012), pp. 57–78, <https://doi.org/10.1007/s11081-011-9159-x>, [10.1007/s11081-011-9159-x](https://doi.org/10.1007/s11081-011-9159-x).
- [44] M. A. SALAZAR DE TROYA, *Letop: level set topology optimization in Firedrake*, <https://github.com/LLNL/letop>.
- [45] C. TALISCHI, G. H. PAULINO, A. PEREIRA, AND I. F. MENEZES, *Polytop: a Matlab implementation of a general topology optimization framework using unstructured polygonal finite element meshes*, *Structural and Multidisciplinary Optimization*, 45 (2012), pp. 329–357, <https://doi.org/10.1007/s00158-011-0696-x>.
- [46] C. TALISCHI, G. H. PAULINO, A. PEREIRA, AND I. F. M. MENEZES, *Polygonal finite elements for*

- topology optimization: A unifying paradigm*, International Journal for Numerical Methods in Engineering, 82 (2010), pp. 671–698, <https://doi.org/10.1002/nme.2763>.
- [47] A. THOMAS, *Discontinuous Galerkin discretised level set methods with applications to topology optimisation*, PhD thesis, Durham University, 2020.
- [48] M. T. TRAN, M. N. NGUYEN, T. Q. BUI, AND H. Q. NGUYEN, *An enhanced proportional topology optimization with virtual elements: Formulation and numerical implementation*, Finite Elements in Analysis and Design, 222 (2023), p. 103958, <https://doi.org/10.1016/j.finel.2023.103958>.
- [49] C. H. VILLANUEVA AND K. MAUTE, *Density and level set-XFEM schemes for topology optimization of 3-D structures*, Comput. Mech., 54 (2014), pp. 133–150, <https://doi.org/10.1007/s00466-014-1027-z>.
- [50] Z. J. WEGERT, J. MANYER, C. MALLON, S. BADIA, AND V. J. CHALLIS, *Gridaptopopt.jl: A scalable julia toolbox for level set-based topology optimisation*, 2024, <https://arxiv.org/abs/2405.10478>.
- [51] P. WEI AND G. H. PAULINO, *A parameterized level set method combined with polygonal finite elements in topology optimization*, Structural and Multidisciplinary Optimization, 61 (2020), pp. 1913–1928, <https://doi.org/10.1007/s00158-019-02444-y>.
- [52] Q. XIA, T. SHI, S. LIU, AND M. Y. WANG, *A level set solution to the stress-based structural shape and topology optimization*, Computers & Structures, 90-91 (2012), pp. 55–64, <https://doi.org/10.1016/j.compstruc.2011.10.009>.
- [53] S. YAMASAKI, T. NOMURA, A. KAWAMOTO, K. SATO, AND S. NISHIWAKI, *A level set-based topology optimization method targeting metallic waveguide design problems*, International Journal for Numerical Methods in Engineering, 87 (2011), pp. 844–868, <https://doi.org/10.1002/nme.3135>.